Structural, Morphological, and Vibrational Studies On $Li(Li_{0.05}Ni_{0.7-x}Mn_{0.25}Fe_x)O_2$ (x=0,0.1,0.3,0.5,0.7) Cathode Material for Li-Ion Batteries

A. Nichelson[1], , , and X.Sahaya Shajan[1,*]
[1] Centre for Scientific and Applied Research,
PSN College of Engineering and Technology,
Tirunelveli-627 152, Tamil Nadu, India.

S. Karthickprabhu[2]
[2] K.Ramakrishnan College of Technology,
Samayapuram, Tiruchirappalli-621112,
Tamilnadu,India

K. Karuppasamy[3]
[3] Polymer Materials Lab,
Department of Chemical and Biomolecular Engineering,
Sogang University,
Mapo gu, Seoul, South Korea

Abstract **- Lithium rich layered $Li(Li_{0.05}Ni_{0.7-x}Mn_{0.25}Fe_x)O_2$ (x = 0,0.1,0.3,0.5,0.7) cathode materials were prepared citric acid assisted sol-gel technique. The prepared samples were subjected to characterization techniques such as X-ray diffraction studies, scanning electron microscopy, energy dispersive spectra analysis, FTIR, Raman spectra. The structural and morphological behavior was studied using XRD and SEM. $Li(Li_{0.05}Ni_{0.7-x}Mn_{0.25}Fe_x)O_2$ possess the hexagonal α-$NaFeO_2$. The crystallite size of the $Li(Li_{0.05}Ni_{0.7-x}Mn_{0.25}Fe_x)O_2$ cathode material were around 50 nm, which supports the movement of lithium ion throughout the material. The metal oxygen interaction of the prepared cathode material was analyzed by FT-IR spectroscopy.**

Keywords - Sol-gel; crystallite; lithium ion batteries; cathode material

1. INTRODUCTION

Lithium ion batteries (LIBs) occupied an important place in the production of electrical appliances for the past two decades. Cellular phones, digital cameras, laptops and LIBs are few of them. These gadgets consumed LIBs due to their excellent properties such as high specific energy, high adoptability and slow discharge rate. Cathode, anode, electrolyte and separator, are the components of LIBs whereas the cathode material with less toxicity and more safety has more impact on to the cost of LIBs [1]. The crystal structure of the cathode material has a significant role because of its necessity for feasible lithium ion movement. The different crystal structure of the cathode materials are olivine, layered and spinel phased structure [2,3]. Owing to high discharge capacity, high electrical conductivity and capacity retention layered cathode materials have opted more for LIBs [4]. Among the layered oxides, the first material which was investigated and implemented as cathode material for LIBs is $LiCoO_2$, and the LIBs with $LiCoO_2$ as cathode and graphite as anode have been developed at a high level. However, the cell performance showed criticality which indeed need some innovations in the materials, both in preparation and performance [5]. Meanwhile, its low thermal stability and high cost is main barrier for large sized cells in hybrid–electric vehicles (HEV).

The usage of $LiMO_2$ (M=Co, Ni, Mn) leads to a new dimension of research with the combination of metal ions in 3d transition state. The reports on lithium–nickel-manganese-cobalt oxides (LNMCs) showing their significance because of their capacity and capacity retention [6] Ohzuku and his co-workers have done a detailed study on $LiNi_{1/3}Co_{1/3}Mn_{1/}3O_2$ [7-10]. Afterwards, various stoichiometric ratios of LNMC have been studied. Amongst them the lithium rich LNMC is in focus due to their good thermal stability and capacity retention [11]. In addition, the surface modification and effect of dopants is being under study. Zn-doped $LiCo_{0.3}Ni_{0.4-x}Mn_{0.3}Zn_xO_2$ cathode materials were synthesized via co-precipitation method by Chen et al. They found that $LiCo_{0.3}Ni_{0.4-x}Mn_{0.3}Zn_xO_2$ had stable layered structure with α-$NaFeO_2$ type with x up to 0.05. Zn-doping has improved the high rate discharge capability and thermal stability [12].Tang et al successfully prepared Titanium doped cathode material $LiNi_{0.8}Co_{0.2-x}Ti_xO_2$ ($0 \le x \le 0.1$) powders with a high tap density [13]. The element substitution such as Al, Fe, Ga, Cr, Mg, Ti instead of cobalt in Lithium manganese nickel cobalt oxide also displayed good results [14]

Various synthesis methods are there to prepare the cathode materials such as co precipitation method, combustion method, sol gel method and solid state reaction method. Solgel method has its own significance in the preparation of cathode material since the materials prepared by this method possess uniform particle size and good stoichiometry [15,16]. In the present study, the compound $Li(Li_{0.05}Ni_{0.7-x}Mn_{0.25}Fe_x)O_2$ compound was prepared by citric acid assisted modified sol-gel method where, citric acid acted as a chelating agent. The chelating agents like citric acid act on nitrate ions to decompose it and the heat evolved from the decomposition of nitrate is utilized to decompose the remaining organic constituents [17]. The cathode material $Li(Li_{0.05}Ni_{0.7-x}Mn_{0.25}Fe_x)O_2$ prepared by sol-gel method has been subjected to subjected to X-ray diffraction (XRD), Scanning electron microscopy (SEM), Fourier Transform Infrared Spectroscopic analysis (FTIR), Energy dispersive analysis by X-rays (EDX) and Raman Spectroscopic analysis. The observed results were discussed and reported herein.

2. EXPERIMENTAL DETAILS

The materials used are of AR grade purchased from Merck. Lithium nitrate ($LiNO_3$), Manganese Nitrate $Mn(NO_3)_2.6H_2O$, Nickel Nitrate $(Ni(NO_3)_2.6H_2O$ and Iron

III nitrate $Fe(NO_3)_3$ $9H_2O$, Citric acid ($C_6H_8O_7$). The cathode material $Li(Li_{0.05}Ni_{0.7-x}Mn_{0.25}Fe_x)O_2$ were prepared by sol-gel method . The precursor materials were dissolved in distilled water and stirred for 7h. Now, citric acid is added as a chelating agent, drop wise to the solution. The pH was maintained between 6 and 7 by the addition of ammonium hydroxide. The solution was heated to 80 ˚C under continuous stirring to form a gel. The gel was preheated to 500 ˚C for 4 h. The obtained powder was grounded well for 2 h and again calcined at 850 ˚C for 15 h.

The powder X-ray diffraction (PANalytical-XPERT PRO, Netherlands) measurement using CuKα radiation was employed to characterize the synthesized material. The morphological behavior and elemental analysis were done using SEM analyzer (JEOL-JSM.6400 with acceleration voltage of 5 kV). The FTIR spectrum was recorded using JASCO FTIR/4100 spectrophotometer (Japan) in the region 400-1100 cm^{-1} at room temperature with a signal resolution of 8 cm^{-1}. The Raman spectra were recorded by Laser Raman Spectroscopy with RENISHAW via Raman microscope using the 514 nm line of Argon laser source

The cathodic material $Li(Li_{0.05}Ni_{0.7-x}Mn_{0.25}Fe_x)O_2$ was prepared by sol-gel method. The crystalline structure of the material is identified using X-ray diffraction. The surface morphology was studied with the help of Scanning electron microscope. The presence of elements in the compounds was identified using EDS analysis. The complexation behaviour of the prepared samples was studied using the FTIR spectroscopy. Raman spectroscopy was used for the phase identification of the samples.

3.1x -Ray Diffraction Studies

The XRD pattern of $Li(Li_{0.05}Ni_{0.7-x}Mn_{0.25}Fe_x)O_2$ calcined at 850 ˚C is shown in Fig.1. The diffraction peaks observed are indexed based on the hexagonal α-$NaFeO_2$ structure with a space group of $R\bar{3}m$ (166) [JCPDS file no 44-0145] [18,19]. This shows the presence of alternate layers of Li atom and MO_6 octahedra (M= Ni, Fe, Mn) indicate pure phase layered crystal structure [20].But the crystalline phase is absent in the case of $Li(Li_{0.05}Ni_{0.7-x}Mn_{0.25}Fe_x)O_2$ with x=0.7.The peak splitting observed near 38˚(006/102) and 65˚(018/110), shows that the layered structure is well developed as reported by Kim et al[21]. In the α-$NaFeO_2$-type structure, the oxygen sub lattice forms a close-packed face centered cubic (fcc) lattice with a distortion in the 'c' direction, results in clear splitting between the (0 0 6)/(1 0 2) and (1 0 8)/(1 1 0) peaks in the XRD patterns. When this distortion in the 'c' direction is absent, the (0 0 6)/(1 0 2) and (1 0 8)/(1 1 0) peaks combine to form single peaks in the XRD pattern [22].

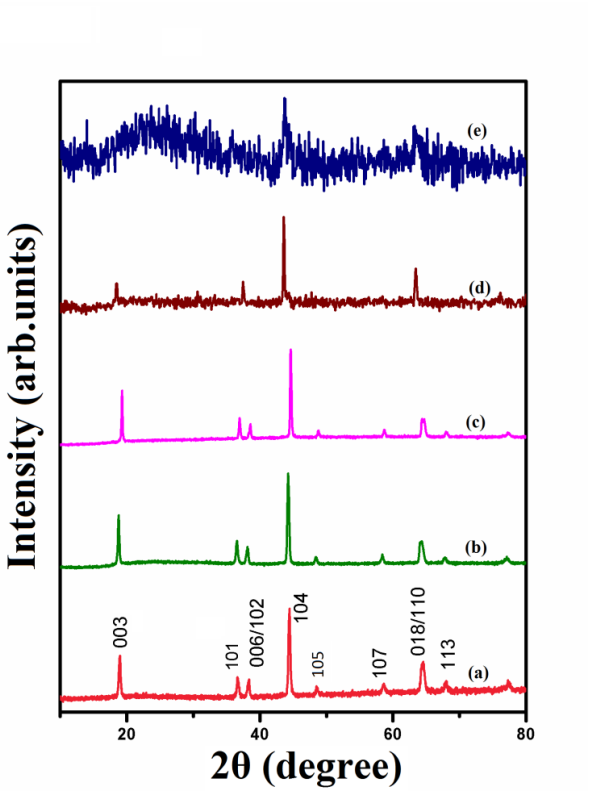

Figure 1: The XRD pattern of $Li(Li_{0.05}Ni_{0.7-x}Mn_{0.25}Fe_x)O_2$ calcined at 850 ˚C

From the X-ray diffraction data, the value of interplanar spacing d_{hkl} was calculated using the Bragg's relation [23] as follows,

$$d_{hkl} = \frac{\lambda}{2sin\theta} \quad (3.1)$$

The lattice parameters a and c were calculated using the equation mentioned below [24].

$$\frac{1}{d^2_{hkl}} = \frac{4}{3}\left[\frac{h^2+hk+k^2}{a^2}\right] + \left[\frac{l^2}{c^2}\right] \quad (3.2)$$

The unit cell is the parallelepiped built on the vectors a, b, c of a crystallographic basis of the direct lattice. Its volume is given by the scalar triple product, V = (a, b, c) and corresponds to the square root of the determinant of the metric tensor[25]. The total volume of the unit cell (V) is calculated using the following Equation (3.3)

$$V = \frac{\sqrt{3}a^2c}{2} \quad (3.3)$$

The lattice parameter a and c value changes with respect to the increase in value of x in the stoichiometric compound $Li(Li_{0.05}Ni_{0.7-x}Mn_{0.25}Fe_x)O_2$ as given in Table .1. The lattice parameters 'a' and 'c' changes with respect to the increase in 'x' value, which is reflected in the c/a ratio and in the unit cell volume 'V'. The intensity ratio of the peaks with lattice planes I_{003} and I_{104} gives the information about cationic mixing in the cathode material. The critical value of I_{003}/ I_{104} ratio is 1.2 for the layer structured material [26]. In general, I_{003}/ I_{104} ratio is less than the critical value, there is significant amount of cationic mixing and the cationic mixing is absent for the I_{003}/ I_{104} values greater than critical value. The ratio of I_{003}/ I_{104} is found to have lower values as the 'x' value increases from 0 to 0.947, which is observed from Table .1.

Table .1. Crystal parameters of $Li(Li_{0.05}Ni_{0.7-x}Mn_{0.25}Fe_x)O_2$ for x = 0,0.1,0.3,0.5,0.7

Sample	Crystallite size(nm)	a(Å)	c(Å)	c/a	V(Å^3)	I_{003}/I_{104}
$Li(Li_{0.05}Ni_{0.7}Mn_{0.25})O_2$	53	2.885	14.07	4.876	101.42	0.947
$Li(Li_{0.05}Ni_{0.6}Mn_{0.25}Fe_{0.1})O_2$	45	2.896	14.160	4.889	102.87	0.557
$Li(Li_{0.05}Ni_{0.4}Mn_{0.25}Fe_{0.3})O_2$	62	2.901	13.799	4.755	100.63	0.591
$Li(Li_{0.05}Ni_{0.2}Mn_{0.25}Fe_{0.5})O_2$	44	2.932	14.407	4.912	107.20	0.261
$Li(Li_{0.05}Mn_{0.25}Fe_{0.7})O_2$	---	--	--	--	--	---

The crystallite size was estimated using Scherrer's formula as given in the following equation,

$$D = \frac{K\lambda}{\beta cos\theta} \quad (3.4)$$

where, the constant K is 0.9, λ is the wavelength of X-ray used (λ = 1.5406 Å), and β is the full width at half- maximum of the diffraction peak corresponding to 2θ. Using above equation the crystallite sizes obtained were found to be in the nanometer range. The crystallite size was measured by taking the average of three main line widths from the XRD patterns. The average crystallite size of the samples calculated using the Scherrer formula is in the range between 44 to 62 nm excluding the sample $Li(Li_{0.05}Mn_{0.25}Fe_{0.7})O_2$, which can be observed from Table .1.

3.2 FTIR SPECTROSCOPIC STUDIES

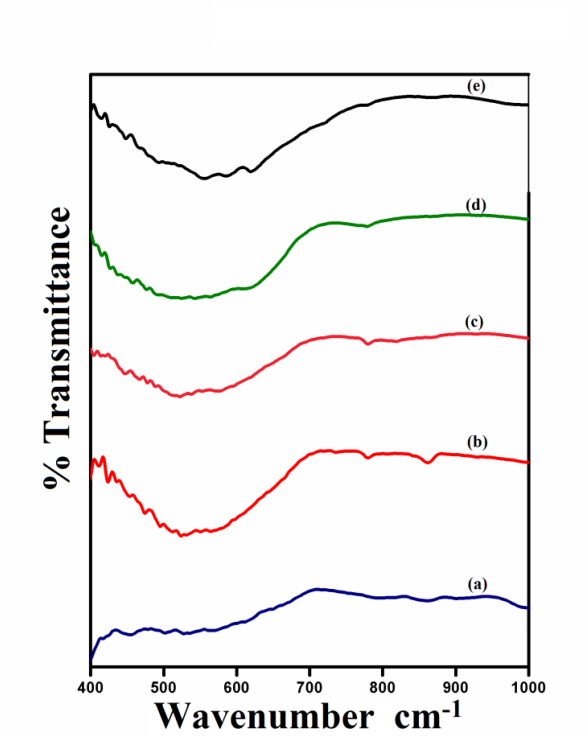

Figure 2: FTIR spectra of $Li(Li_{0.05}Ni_{0.7-x}Mn_{0.25}Fe_x)O_2$ (a) x = 0 (b) x = 0.1 (c) x = 0.3 (d) x = 0.5 (e) x = 0.7

The vibrational spectra of the samples $Li(Li_{0.05}Ni_{0.7-x}Mn_{0.25}Fe_x)O_2$ synthesized were recorded in the wave number range 400 - 4000 cm^{-1}. In this study the metal oxide peaks are expected to be present in the range between 400 and 1000 cm^{-1} and the same is presented in Fig.2. The strong peak are obtained at 570 cm^{-1}, 568 cm^{-1}, 576 cm^{-1}, 618 cm^{-1}, 620 cm^{-1} respectively for the synthesized material $Li(Li_{0.05}Ni_{0.7-x}Mn_{0.25}Fe_x)O_2$ with (i) x = 0 (ii) x = 0.1 (iii) x = 0.3 (iv) x = 0.5 (v) x = 0.7.

The corresponding values are assigned to asymmetric stretching modes of M-O (M = Ni/ Fe/ Mn). The peak shift in the spectra may be due to the increase in elemental concentration of Iron. The weak peaks obtained around 530 cm^{-1} may be ascribed to Li-O stretch which suggests the presence of Li in the material. Further, a peak in the far infra-red region 271 cm^{-1} is expected, but it was not covered in the present study. Moreover, the corresponding less intense peaks observed at 419 cm^{-1} , 421 cm^{-1} , 418 cm^{-1} , 413 cm^{-1} and 415 cm^{-1} in Fig.2 (a-e) could be assigned to the bending modes of O-M-O chemical bonds [27,28]. The corresponding peaks mentioned in Fig.2 (b-e) are also correlate with the values of Fe-O stretching and bending modes [29]. From the vibrational spectra analysis, it is concluded that, there is a good interaction between metal and oxygen.

3.3Raman Spectroscopy Analysis

Raman spectroscopy of the prepared samples has been analyzed using Renishaw InVia Raman spectro photometer. Raman spectra of Li $(Li_{0.05}Ni_{0.7-x}Mn_{0.25}Fe_x)O_2$ samples prepared at various compositions are shown in Fig.3.

It is observed from Figure 3.3(a-e) the observation of peaks around 575 cm^{-1} and 480 cm^{-1} may correspond to the Metal Oxide symmetric stretching and bending modes, respectively. For the layered structure cathode material with a space group $R\bar{3}m$ which is similar to the compound $LiCoO_2$ [30].

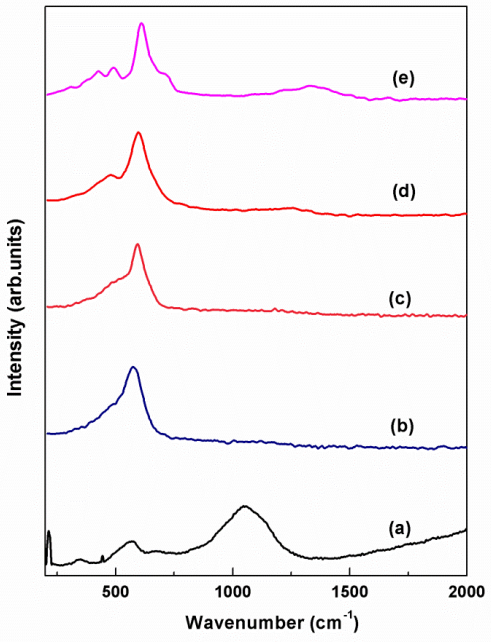

Figure 3: Raman spectra of $Li(Li_{0.05}Ni_{0.7-x}Mn_{0.25}Fe_x)O_2$ (a) x = 0 (b) x = 0.1 (c) x = 0.3 (d) x = 0.5 (e) x = 0.7.

Therefore the corresponding optical vibration modes are: $\Gamma = A_{2g} + E_g + 2A_{2u} + 2E_u$ [31]. The first two modes are visible only by Raman while the second two modes can be seen by IR. Theoretically, two Raman bands and four IR bands should be visible for the layer structured material with space group $R\bar{3}m$. Fig.3(a-c) shows the peaks around 575 cm^{-1} and 480 cm^{-1} which corresponds to the active M-O symmetrical stretching and bending vibrational Raman modes of A_{1g} and E_g. The samples are clearly showing the two active Raman modes except the compounds with x = 0 and x = 0.7, which shows additional peaks other than the two modes. The additional peaks observed for the Li $(Li_{0.05}Ni_{0.7-x}Mn_{0.25}Fe_x)O_2$ compound with x = 0 reflects the display of single peak at the 2θ values 38˚ and 68˚. This may correspond to the cubical sub lattice of oxygen in the α-$NaFeO_2$ type structure. For x = 0.7, the humps observed around 420 cm^{-1} may be due to the absence of nickel in the compound [32].

3.4 Scanning Electron Microscope And Energy Dispersive Analysis

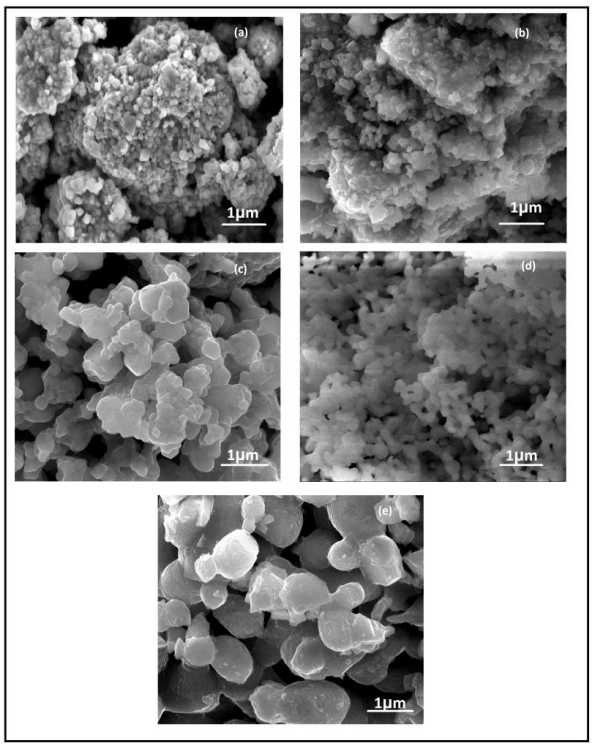

Figure 4: SEM images of $Li(Li_{0.05}Ni_{0.7-x}Mn_{0.25}Fe_x)O_2$ (a) x = 0 (b) x = 0.1 (c) x = 0.3 (d) x = 0.5 (e) x = 0.7

Surface morphology of $Li(Li_{0.05}Ni_{0.7-x}Mn_{0.25}Fe_x)O_2$ was studied by scanning electron microscopy. SEM image of $Li(Li_{0.05}Ni_{0.7-x}Mn_{0.25}Fe_x)O_2$ is presented in Fig.4. The agglomeration of particles is more in the $Li(Li_{0.05}Ni_{0.7-x}Mn_{0.25}Fe_x)O_2$ for x = 0.7 as it is non crystalline as observed from the XRD pattern. Similar pattern of particles are observed for the samples $Li(Li_{0.05}Ni_{0.7-x}Mn_{0.25}Fe_x)O_2$ (x = 0, 0.1, 0.3 and 0.5). Furthermore, the particles are observed to be formed in different sizes mostly in the range of 200-250 nm for the samples mentioned in Fig .4 (a-d).

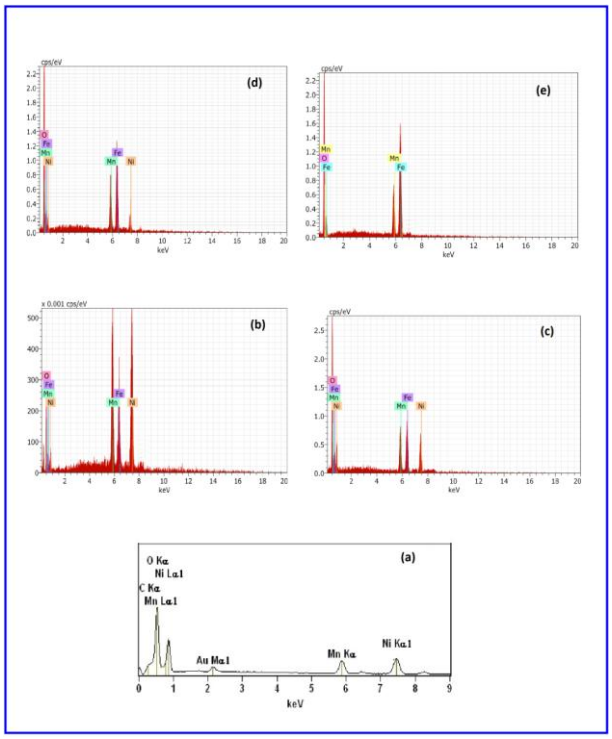

Figure 5: Energy Dispersive Spectra of $Li(Li_{0.05}Ni_{0.7-x}Mn_{0.25}Fe_x)O_2$ (a) x = 0 (b) x = 0.1 (c) x = 0.3 (d) x = 0.5 (e) x = 0.7

The addition of citric acid as chelating agent, while preparing the precursor leads to the even distribution of particles, which in turn helps to keep the particle size small after calcination. The large surface area of the material will be obtained from smaller particle size, which could shorten the diffusion path of lithium ion and be helpful to improve the electrochemical performance of the cathode material [33]. The EDS spectra of the synthesized $Li(Li_{0.05}Ni_{0.7-x}Mn_{0.25}Fe_x)O_2$ are presented in Fig.5.

The spectra confirm the presence of Ni, Mn, Co and O in the prepared samples. Lithium is not detected in the EDS spectrum due to its low atomic number [34]

CONCLUSION

XRD analysis of $Li(Li_{0.05}Ni_{0.7-x}Mn_{0.25}Fe_x)O_2$ (x=0,0.1,0.3,0.5,0.7) possessed layered hexagonal α-$NaFeO_2$ structure. The crystallite size of the samples was between 44 – 62 nm. From FTIR and Raman spectroscopic analysis it was observed that the samples exhibit the vibrational modes of asymmetric stretching of M-O and bending modes of O-M-O revealed the formation of layered structure compounds. In FTIR spectra the peaks appeared between 420 cm^{-1} & 450 cm^{-1} were allotted to the asymmetric stretching mode of M-O and the peaks between 570 cm^{-1} & 650 cm^{-1} were attributed to the bending modes of O-M-O. Whereas in Raman spectroscopy it displayed two Raman modes of vibration around 480 cm^{-1} & 575 cm^{-1} were assigned to the stretching and bending modes of metal and oxygen except the lower and higher values of x. The SEM analysis showed a good morphological behaviour and the particle sizes between 200 – 300 nm which favours the lithium ion motion. EDS displayed the presence of elements in the corresponding compounds.

REFERENCES

[1] Tarascon J-M, Armand M (2001) Issues and challenges facing rechargeable lithium batteries. Nature 414 (6861),359-367

[2] Fergus JW (2010) Recent developments in cathode materials for lithium ion batteries. Journal of Power Sources 195 (4):939-954

[3] Nichelson A, Karthickprabhu S, Karuppasamy K, Hirankumar G, Sahaya Shajan X 2016 A Brief Review on Integrated (Layered and Spinel) and Olivine Nanostructured Cathode Materials for Lithium Ion Battery Applications. Materials Focus 5 (4):324-334

[4] Whittingham, MS, 'Lithium batteries and cathode materials', Chemical reviews, 2004,104,(10), 4271-4302

[5] Ohzuku, T., Nagayama, M., Tsuji, K., & Ariyoshi, K. (2011). High-capacity lithium insertion materials of lithium nickel manganese oxides for advanced lithium-ion batteries: toward rechargeable capacity more than 300 mA hg− 1. *Journal of Materials chemistry*, *21*(27), 10179-10188.

[6] Rajarathinam, S., Mitra, S., & Petla, R. K. (2013). Li 2 MnO 3 rich-LiMn 0.33 Co 0.33 Ni 0.33 O 2 integrated nano-composites as high energy density lithium-ion battery cathode materials. *Electrochimica Acta*, *108*, 135-144.

[7] Yoshizawa, H., & Ohzuku, T. (2007). An application of lithium cobalt nickel manganese oxide to high-power and high-energy density lithium-ion batteries. *Journal of Power Sources*, *174*(2), 813-817.

[8] Ohzuku, T., & Makimura, Y. (2001). Layered lithium insertion material of LiCo1/3Ni1/3Mn1/3O2 for lithium-ion batteries. *Chemistry Letters*, *30*(7), 642-643.

[9] Yabuuchi, N., & Ohzuku, T. (2003). Novel lithium insertion material of LiCo 1/3 Ni 1/3 Mn 1/3 O 2 for advanced lithium-ion batteries. *Journal of Power Sources*, *119*, 171-174.

[10] Koyama Y, Tanaka I, Adachi H, Makimura Y, Ohzuku T (2003) Crystal and electronic structures of superstructural $Li_{1-x}[Co_{1/3}Ni_{1/3}Mn_{1/3}]O_2$(0≤< i> x</i>≤ 1)). Journal of Power Sources 119:644-648.

[11] Yan, J., Liu, X., & Li, B. (2014). Recent progress in Li-rich layered oxides as cathode materials for Li-ion batteries. *Rsc Advances*, *4*(108), 63268-63284.

[12] Chen, Y, Ruizhen, C, Tang, Z & Wang, L 2009, 'Synthesis and characterization of Zn-doped $LiCo_{0.3}Ni_{0.4}$-$xMn_{0.3}Zn_xO_2$ cathode materials for lithium-ion batteries', Journal of Alloys and Compounds, 476, (1), 539-542

[13] Tang, H, Zhao, F, Chang, ZR, Yuan, XZ & Wang, H 2009, 'Synthesis and Electrochemical Properties of High Density $LiNi_{0.8}Co_{0.2-x}Ti_xO_2$ for Lithium-Ion Batteries', Journal of the electrochemical society, 156,(6), A478-A482

[14] Wang, CC & Manthiram, A 2013, 'Influence of cationic substitutions on the first charge and reversible capacities of lithium-rich layered oxide cathodes', Journal of Materials Chemistry A,(1),(35), 10209-10217

[15] Nichelson A, Thanikaikarasan S, Kollu P, Sebastian P, Mahalingam T, Shajan XS (2014) Structural, Morphological and Impedance Spectroscopic Analyses of Nano Li (Li0. 05Ni0. 4Co0. 3Mn0. 25) O-2 Cathode Material Prepared by Sol-Gel Method. Journal of New Materials for Electrochemical Systems 17 (3):153-158

[16] Fu, L. J., Liu, H., Li, C., Wu, Y. P., Rahm, E., Holze, R., & Wu, H. Q. (2005). Electrode materials for lithium secondary batteries prepared by sol–gel methods. *Progress in Materials Science*, *50*(7), 881-928.

[17] Hwang, B. J., Santhanam, R., & Liu, D. G. (2001). Characterization of nanoparticles of LiMn 2 O 4 synthesized by citric acid sol–gel method. *Journal of power sources*, *97*, 443-446.

[18] Laha S, Morán E, Sáez-Puche R, Alario-Franco M, Dos santos-Garcia A, Gonzalo E, Kuhn A, Natarajan S, Gopalakrishnan J, Garcia-Alvarado F (2013) Li 3 MRuO 5 (M= Co, Ni), new lithium-rich layered oxides related to LiCoO 2: promising electrochemical performance for possible application as cathode materials in lithium ion batteries. Journal of Materials Chemistry A 1 (36):10686-10692

[19] Hewston TA, Chamberland B (1987) A survey of first-row ternary oxides LiMO 2 (M= Sc-Cu). Journal of Physics and Chemistry of Solids 48 (2):97-108

[20] Jeong SK, Song C-H, Nahm KS, Stephan AM (2006) Synthesis and electrochemical properties of Li [Li0. 07Ni0. 1Co0. 6Mn0. 23] O2 as a possible cathode material for lithium-ion batteries. Electrochimica acta 52 (3):885-891

[21] Kim H-S, Kong M, Kim K, Kim I-J, Gu H-B (2007) Effect of carbon coating on LiNi< sub> 1/3</sub> Mn< sub> 1/3</sub> Co< sub> 1/3</sub> O< sub> 2</sub> cathode material for lithium secondary batteries. Journal of Power Sources 171 (2):917-921

[22] Gao Y, Yakovleva M, Ebner W (1998) Novel LiNi1− x Ti x/2Mg x/2 O 2 Compounds as Cathode Materials for Safer Lithium-Ion Batteries. Electrochemical and solid-state letters 1 (3):117-119

[23] Kittel C, McEuen P (1976) Introduction to solid state physics, vol 8. Wiley New York,

[24] Thanikaikarasan S, Mahalingam T, Sundaram K, Kathalingam A, Kim YD, Kim T (2009) Growth and characterization of electrosynthesized iron selenide thin films. Vacuum 83 (7),1066-1072

[25] Prince E, Wilson AJC, Hahn T, Shmueli U (1999) International tables for crystallography. International Union of Crystallography.

[26] Valanarasu S, Chandramohan R, Somasundaram R, Srikumar S (2011) Structural and electrochemical properties of Eu-doped LiCoO2. Journal of Materials Science: Materials in Electronics 22 (2),151-157

[27] Suresh, P, Rodrigues, S, Shukla, A, Vasan, H & Munichandraiah, N 2005, 'Synthesis of $LiCo_{1-x}Mn_xO_2$ from a low-temperature route and characterization as cathode materials in Li-ion cells', Solid State Ionics, 176,(3), 281-290

[28] Julien C, Camacho-Lopez M, Mohan T, Chitra S, Kalyani P, Gopukumar S (2000) Combustion synthesis and characterization of substituted lithium cobalt oxides in lithium batteries. Solid State Ionics 135 (1),241-248

[29] Sahoo, S, Agarwal, K, Singh, A, Polke, B & Raha, K 2010, ' Characterization of γ-and α-Fe 2 O 3 nano powders synthesized by emulsion precipitation-calcination route and rheological behaviour of α-Fe_2O_3', International Journal of Engineering, Science and Technology, 2(8), 118-126

[30] Gu, Y, Chen, D & Jiao, X 2005, ' Synthesis and electrochemical properties of nanostructured LiCoO2 fibers as cathode materials for lithium-ion batteries', The Journal of Physical Chemistry B, 109, (38), 17901-17906

[31] Huang W, Frech R (1996) Vibrational spectroscopic and electrochemical studies of the low and high temperature phases of LiCo 1− x M x O 2 (M= Ni or Ti). Solid State Ionics 86:395-400

[32] Riley LA, Van Atta S, Cavanagh AS, Yan Y, George SM, Liu P, Dillon AC, Lee S-H (2011) Electrochemical effects of ALD surface modification on combustion synthesized LiNi 1/3 Mn 1/3 Co 1/3 O 2 as a layered-cathode material. Journal of Power Sources 196 (6):3317-3324

[33] Zheng, J, Wu, X & Yang, Y 2011, 'A comparison of preparation method on the electrochemical performance of cathode material Li $[Li_{0.2}Mn_{0.54}Ni_{0.13}Co_{0.13}]O_2$ for lithium ion battery', Electrochimica acta, 56, (8), 3071-3078

[34] Jin X, Xu Q, Yuan X, Zhou L, Xia Y (2013) Synthesis, characterization and electrochemical performance of Li [Li 0.2 Mn 0.54 Ni 0.13 Co 0.13] O 2 cathode materials for lithium-ion batteries. Electrochimica acta 114,605-610